Hierarchy of multiple many-body interaction scales in high-temperature superconductors

W. Meevasana,[1,*] X. J. Zhou,[1,2] S. Sahrakorpi,[3] W. S. Lee,[1] W. L. Yang,[1,2] K. Tanaka,[1,2] N. Mannella,[1,2] T. Yoshida,[1,4] D. H. Lu,[1] Y. L. Chen,[1] R. H. He,[1] Hsin Lin,[3] S. Komiya,[5] Y. Ando,[5] F. Zhou,[6] W. X. Ti,[6] J. W. Xiong,[6] Z. X. Zhao,[6] T. Sasagawa,[1,7] T. Kakeshita,[7] K. Fujita,[7] S. Uchida,[7] H. Eisaki,[8] A. Fujimori,[4] Z. Hussain,[2] R. S. Markiewicz,[3] A. Bansil,[3] N. Nagaosa,[7] J. Zaanen,[9] T. P. Devereaux,[10] and Z.-X. Shen[1,2,†]

[1]*Department of Physics, Department of Applied Physics, and Stanford Synchrotron Radiation Laboratory, Stanford University, Stanford, California 94305, USA*

[2]*Advanced Light Source, Lawrence Berkeley National Laboratory, Berkeley, California 94720, USA*

[3]*Physics Department, Northeastern University, Boston, Massachusetts 02115, USA*

[4]*Department of Complexity Science and Engineering, University of Tokyo, Kashiwa, Chiba 277-856, Japan*

[5]*Central Research Institute of Electric Power Industry, Iwato-kita, Komae, Tokyo 201–8511, Japan*

[6]*National Laboratory for Superconductivity, Institute of Physics, Chinese Academy of Sciences, Beijing 100080, China*

[7]*CREST, Department of Applied Physics, Department of Advanced Materials Science, and Department of Superconductivity, University of Tokyo, Bunkyo-ku, Tokyo 113–8656, Japan*

[8]*Nanoelectronic Research Institute, AIST, Tsukuba 305-0032, Japan*

[9]*The Instituut-Lorentz for Theoretical Physics, Leiden University, Leiden NL-2300 RA, The Netherlands*

[10]*Department of Physics, University of Waterloo, Waterloo, Ontario, Canada N2L 3G1*

(Received 20 December 2006; published 9 May 2007)

To date, angle-resolved photoemission spectroscopy has been successful in identifying energy scales of the many-body interactions in correlated materials, focused on binding energies of up to a few hundred meV below the Fermi energy. Here, at higher-energy scale, we present improved experimental data from four families of high-T_c superconductors over a wide doping range that reveal a hierarchy of many-body interaction scales focused on: the low-energy anomaly ("kink") of 0.03–0.09 eV, a high-energy anomaly of 0.3–0.5 eV, and an anomalous enhancement of the width of the local-density-approximation-based CuO_2 band extending to energies of ≈2 eV. Besides their universal behavior over the families, we find that all of these three dispersion anomalies also show clear doping dependence over the doping range presented.

DOI: 10.1103/PhysRevB.75.174506 PACS number(s): 74.72.−h, 79.60.−i

I. INTRODUCTION

Many-body interaction is a key to understanding novel properties of quantum matter. As an extreme example, the complexity due to charge, spin, and lattice interactions in high-T_c superconductors makes it difficult to identify the essential microscopic ingredients for the basic model—a reason behind the current debate on the mechanism. The energy-momentum dispersion relationship measured by angle-resolved photoemission spectroscopy (ARPES) provides an excellent tool for identifying these scales. Energy scales where these interactions are manifested usually provide important insights into the nature of the interactions. At an early stage, APRES proved to be successful in identifying the energy scale of the *d*-wave gap in high-T_c superconductors.[1,2] To date, a focus of the discussion in ARPES has been on the nature of electron-boson coupling, which manifests itself in the form of the low-energy anomaly ("kink") near 0.03–0.09 eV.[2–10] However, little attention has been paid to the features at higher binding energies.

Given the strong many-body interactions and complex band structure, one expects only incoherent features and complex spectral weight modulation at high energy. The fact that one can see neatly defined momentum dependent features which are robust against doping and measuring conditions (e.g., photon energy) is unexpected and thus provides a new opportunity to understand many-body effects beyond what have traditionally been the points of focus by ARPES, other than some early work on oxygen *p* bands.[11,12] Here, we report ARPES experiments on four families of high-T_c cuprates over a wide range of dopings: $Bi_2Sr_2CuO_6$ (Bi2201), $Bi_2Sr_2CaCu_2O_8$ (Bi2212), $Ba_2Ca_3Cu_4O_8(O_\delta,F_{1-\delta})_2$ (F0234), and $La_{2-x}Sr_xCuO_4$ (LSCO). All of their measured energy-momentum dispersion relationships reveal the simultaneous presence of three energy scales, marked as 1–3 in Fig. 1(d): (1) the band bottom at nearly 2 eV in optimally doped Bi2201, which is deeper than predicted by local-density-approximation (LDA) calculation, (2) the high-energy anomaly (HEA) at ≈0.3–0.5 eV (arrow 2), and (3) the low-energy kink (LEK) near 70 meV (arrow 3) which can be better seen in an enlarged energy window. Various aspects of these energy scales, including the peculiar doping-dependent effects, will be discussed to obtain insights on many-body interactions and their interplay in cuprates.

II. EXPERIMENT AND LDA CALCULATION

We have measured four families of high-T_c cuprates: $Bi_2Sr_2CuO_6$ (Bi2201), $Bi_2Sr_2CaCu_2O_8$ (Bi2212), $Ba_2Ca_3Cu_4O_8(O_\delta,F_{1-\delta})_2$ (F0234),[14] and $La_{2-x}Sr_xCuO_4$ (LSCO). The Bi2201 samples are optimally doped at T_c =35 K and nonsuperconducting overdoped. The Bi2212 samples are optimally doped at T_c=92 K and overdoped at T_c=65 K. The F0234 samples are of T_c=60 K, and the LSCO samples have a wide range of dopings: x=0.03, 0.05, 0.063, 0.07, 0.075, 0.09, 0.12, 0.15, 0.22, and 0.3. The mea-

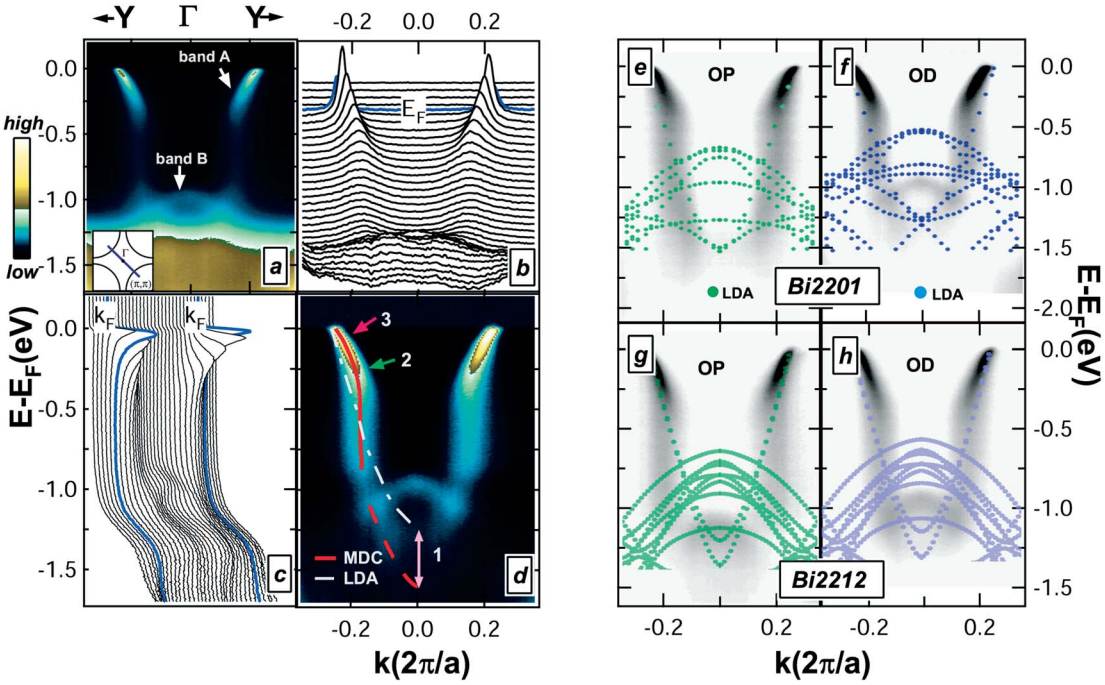

FIG. 1. (Color online) (a) Raw ARPES spectrum, along (0, 0) to (π,π) direction, of nonsuperconducting overdoped Bi2201 at $T=30$ K, while (b) and (c) represent its MDCs and EDCs, respectively. (d) The raw data are normalized with angle-integrated EDC profile for clearer view and the numbers 1–3 mark the wider bandwidth and the high- and low-energy anomalies, respectively. Normalized ARPES spectra are compared with LDA calculations as follows: (e) OP Bi2201 with $T_c=35$ K ($T=45$ K), (f) OD Bi2201, nonsuperconducting ($T=30$ K), (g) OP Bi2212 with $T_c=96$ K ($T=110$ K, LDA from Ref. 13), and (h) OD Bi2212 with $T_c=65$ K ($T=76$ K). Inset in (a) shows the momentum space of the data. Note that the LDA bands in panel (h) are obtained by rigidly shifting the bands in (g) to account for the correct doping level. It is not clear if feature B should be matched to the top of the band structure in (e) or (f) at Γ; however, this uncertainty is not important for our argument, which requires only a relative shift in going from the OP to the OD case.

surements were carried out on beamline 10.0.1 at the ALS, using a Scienta R4000 electron energy analyzer. This analyzer has the advantage of a large-angle window which can cover the band dispersion across the Brillouin zone as shown in Fig. 1. We stress that the wide angle scan allowed us to record the above data without resorting to manual symmetrization. The photon energies are 37, 40, 41, 42, 43, 44, 45, and 55 eV. The energy resolution between 12 and 20 meV was used for various measurements on different samples, and the angular resolution is 0.3°. The samples were cleaved *in situ* at a base pressure better than 4×10^{-11} torr. The samples were measured both in normal and superconducting states.

LDA results here are based on full-potential well-converged computations for the appropriate lattice structures, described in greater detail in Refs. 13 and 15.

III. RESULTS

Figure 1(a) shows the raw ARPES image of the strongly overdoped Bi2201 sample, while its raw momentum-distribution curves (MDCs) and energy-distribution curves (EDCs) are shown in Figs. 1(b) and 1(c), respectively. To see the band near the bottom more clearly, the raw ARPES image is divided by its profile of angle-integrated EDC,[16] as shown in Fig. 1(d); this procedure will not change the MDC-peak position at any given energy. We also note that this renormalization procedure which is used in Figs. 1(d)–1(h) and 2 is only for the purpose of displaying the lower- and higher-energy features together, since, otherwise, the intensity at the higher-energy region will be too high to have a reasonable displaying contrast. The raw data without this renormalization procedure can be seen in Figs. 1(a)–1(c) and 6(a)–6(i).

As marked by numbers 1–3 in Fig. 1(d), we will focus on how our data reveal the simultaneous presence of three energy scales as follows.

A. Anomalous enhancement of the LDA-based CuO_2 bandwidth

As shown in Figs. 1(e)–1(h), ARPES spectra of optimally doped (OP) and overdoped (OD) samples of Bi2201 and Bi2212 systems are overlaid on the corresponding LDA calculations. As seen in all measured samples, the first peculiar feature, especially at lower doping, is that the ARPES bandwidth is found to be wider than LDA calculation. This is anomalous as one expects interactions to enhance the mass and reduce the bandwidth. By extrapolating the band [e.g., the dashed line in Fig. 1(d)], one can get an estimate of the bandwidth that is suitable for qualitative discussion. With doping, the discrepancy between the bandwidths obtained from ARPES and LDA seems to be reduced.

Additional evidence that these high-energy dispersions still contain useful information comes from band B in Fig.

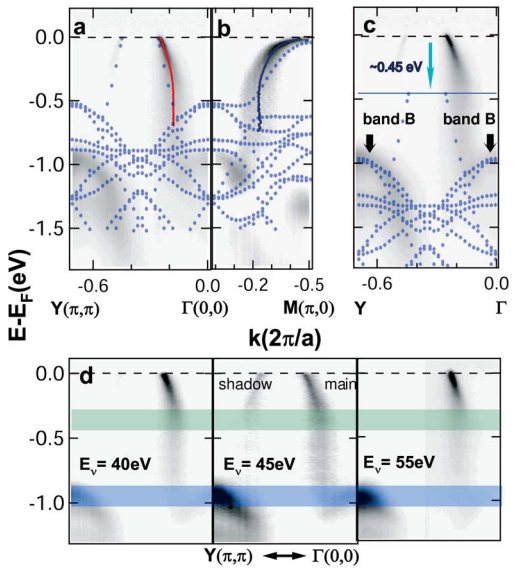

FIG. 2. (Color online) The comparison of normalized ARPES spectra and LDA calculations along (a) (π,π) to (0,0) or nodal direction and (b) (0,0) to $(\pi,0)$ or antinodal direction in OD nonsuperconducting Bi2201 system. (c) shows the agreement of ARPES spectrum and LDA calculation of high-energy band when shifting the LDA by 450 meV to the higher energy. (d) The comparison of the spectra at photon energies E_ν=40, 45, and 55 eV where the upper shaded region denotes the energy scale of HEA and the lower shaded region indicates the top of band B. We note that for E_ν=55 eV, due to the matrix element effect, the intensity of the left band B is large, and therefore we have adjusted the color scale so that we can see the energy scales of both bands A and B clearly.

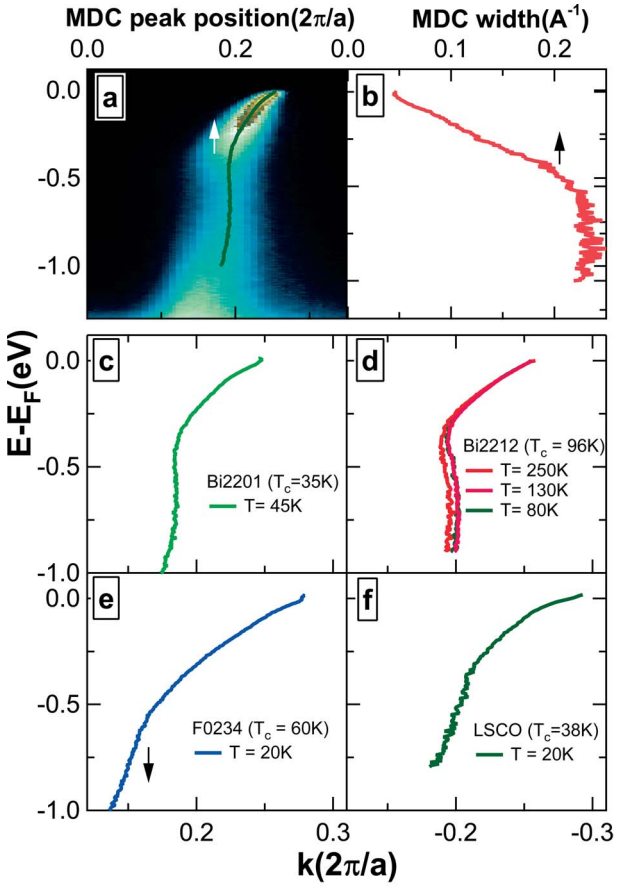

FIG. 3. (Color online) (a) shows MDC-peak dispersion plotted on top of ARPES spectrum and (b) shows corresponding MDC width in OP Bi2201 system (T_c=35 K). (c)–(f) show the MDC-derived dispersions of Bi2201 (T_c=35 K), Bi2212 (T_c=96 K), LSCO (T_c=38 K), and F0234 (T_c=60 K), respectively. Additionally, the temperature dependence of Bi2212 and LSCO dispersions is shown in (d) and (f).

1(a), which shows a maximum at Γ point near 1 eV. This band has a correspondence to an LDA band and thus provides confidence in the data at higher-energy scales, which has been largely unexplored in the cuprates. From the LDA calculation with orthorhombic distortion, this band is the band at Y point [left arrow, Fig. 2(c)], which is folded around the $(\pi/2,\pi/2)$ point. We then compare the LDA and ARPES top part of this band B at Γ point by shifting the LDA band down. A good agreement of ARPES and LDA of this concave-down band [see Fig. 2(c)] can be obtained if the LDA is shifted down ≈0.45 eV for OD Bi2201 sample, and the shifted energy increases to ≈0.8 eV for OP Bi2201 sample,[17] leading to a filled bandwidth near 2 eV. A similar behavior is also observed in the Bi2212 system[17] [Fig. 1(g) and 1(h)]. This bandwidth enhancement was also seen earlier in undoped $Ca_2CuO_2Cl_2$ (CCOC) as its high-energy dispersion matches with the LDA calculation shifted by 0.7 eV.[18]

B. High-energy anomaly of 0.3–0.5 eV

Next, we discuss the high-energy anomaly (HEA) near 0.3–0.5 eV. We extract the MDC-peak position by fitting to Lorentzian curves, as shown by the red and blue curves in Figs. 2(a) and 2(b). We note that especially at high binding energy, MDC-peak position may not represent the real dispersion. As explained in the Appendix, a full two-dimensional (2D) analysis, which directly extracts the spectral function $A(k,\omega)$ and matrix element term separately at once, can avoid the problem of the MDC or EDC analysis alone. However, since the kinklike structure is so large, the MDC-derived dispersion should be able to approximately identify the energy scale of the HEA. To check the three-dimensional behavior of bands A and B, we perform the measurements at various photon energies of 40, 41, 42, 43, 44, 45, and 55 eV, probing different perpendicular momenta k_z. As shown in Fig. 2(d), we find that HEA scale and the top of band B are not very sensitive to the photoenergies, while these energy scales in our LDA calculations do not show strong k_z dependence.

This HEA is present in various cuprate families. While earlier seen in undoped CCOC,[18] the MDC-peak-position graphs of Bi2201, Bi2212, LSCO, and F0234 plotted in Fig. 3 reveal its universality. The energy scales are around 0.3–0.4 eV in Bi2201, Bi2212, and LSCO while around 0.5–0.6 eV in F0234 (for electron-doped band). HEA persists in both superconducting and nonsuperconducting samples, albeit its strength depends on doping. Figure 4 shows the plots of MDC-peak position of LSCO samples which cover a wide doping range of x=0.03–0.30. From the

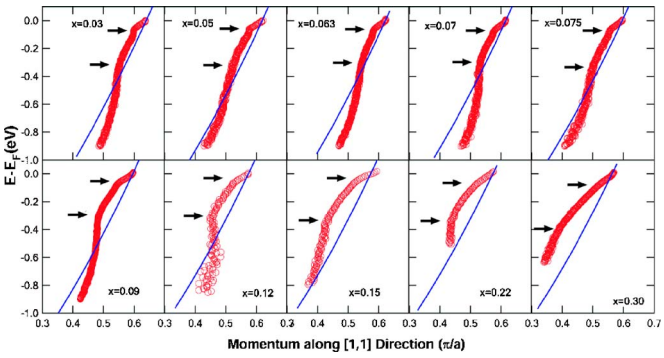

FIG. 4. (Color online) The doping dependence of high-energy dispersion (circles) in LSCO system at $T=20$ K at doping $x=0.03-0.30$. LDA curves for various dopings (lines) are obtained by appropriate rigid shifts of the computations for $x=0$.

figure, the HEA energy does not change much with doping. However, if we define the size of HEA to be the difference between the MDC-derived and LDA dispersions, it increases upon doping in this range. Similar doping-dependent behavior is also observed in Bi2201 and Bi2212 samples which cover a narrower range of doping. For superconducting samples, the HEA persists above and below T_c. Consistent with ARPES data, from in-plane optical conductivity of Bi2212,[19] Norman and Chubukov recently report that the real part of the self-energy is large with a maximum value around 0.3–0.4 eV.[20]

C. Low-energy kink of 0.03–0.09 eV

Finally, the low-energy kink (LEK) around 0.03–0.09 eV is indicated with arrows in Fig. 2(d) and with upper arrows in Figs. 4 and 5(a). Since this feature has been already discussed with regard to the interaction of electron to sharp bosonic mode(s),[2–10] we will not go into the details of this feature, except commenting upon its interesting doping dependence. For LEK, the size of this feature, which is interpreted as strength of electron-boson coupling, reduces upon doping in LSCO (Ref. 9) and Bi2201,[10] while the size of HEA defined previously increases upon doping. It is then intriguing to ask whether an interplay of these two scales of low- and high-energy anomalies will affect our understanding of the doping-dependent effects seen in cuprates.

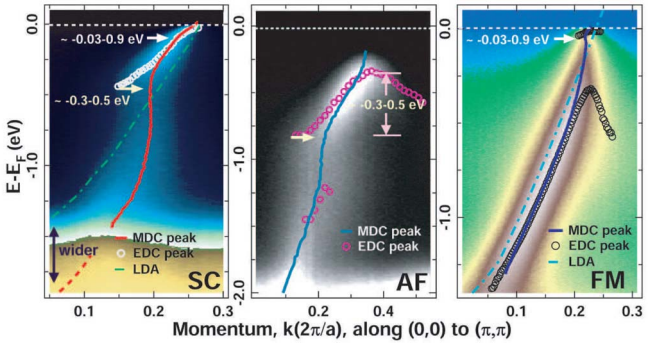

FIG. 5. (Color online) Comparison of electronic structures of three perovskites in (a) superconducting (SC), (b) antiferromagnetic (AF), and (c) ferromagnetic (FM) phases. The images show ARPES data of (a) optimally doped Bi2201, (b) undoped CCOC, and (c) LSMO.

IV. DISCUSSION

The presence of three energy scales in the same data set hints at the hierarchy of interactions that are important to the dynamics of electrons in cuprates. Aside from LEK which we believe is caused by electron-phonon interaction,[6,8–10] HEA and the expanded bandwidth are observations that require more discussion.

To gain more insights into the nature of the energy scales observed, Fig. 5 compares the data of the superconducting (SC) sample, OP Bi2201, with that of the antiferromagnetic (AF) parent compound CCOC and ferromagnetic (FM) $La_{1.2}Sr_{1.8}Mn_2O_7$ (LSMO). Comparison of LSMO and cuprates may give us some insight, since LSMO is reported to have similar pseudogap behavior.[21] The LSMO comparison yields two insights: (i) HEA is probably related to antiferromagnetism as it is absent in the ferromagnetic state and (ii) the LDA calculation appears to give a correct bandwidth if antiferromagnetism is not present. As for LEK near 0.03–0.09 eV, it is seen in metallic cuprates and LSMO but not in insulating CCOC where the polaron effect is too strong, thus suppressing the quasiparticle weight dramatically.[22]

HEA may be related to the short-range Coulomb interaction as in the Hubbard (or *t-J*) model. Calculations using these models show that in undoped $Sr_2CuO_2Cl_2$, the quasiparticle bandwidth of the part below HEA is set by the J scale to be around 2–3 $J\simeq 0.25-0.35$ eV,[23] while the higher-energy part is presumed to be the incoherent bandwith t scale.[18] HEA in the Hubbard calculation, which may come from the meeting of the quasiparticle band and the incoherent lower-Hubbard band, can be seen from the slightly underdoped to overdoped regime;[24] however, a further check still remains in the small doping regime where the calculation is challenging. In $SrVO_3$, a feature similar to HEA is seen in ARPES (Ref. 25) and in LDA+DMFT calculation.[26] With these models, the size of HEA is expected to be less pronounced upon doping,[27] which is opposite to the doping effect we see in Fig. 4.

One possible way to understand the anomalous doping dependence could be the interplay between electron-electron and electron-phonon interactions. This drives the system into the polaronic regime in the underdoped samples,[22] making a quantitative analysis of the size of the HEA difficult because obtaining polaronic physics correctly via an MDC analysis is challenging. Since the polaron physics is very strong in lightly doped regime, this may artificially suppress the HEA size.

Another possibility is that HEA comes from the renormalization effect by bosonic mode(s). The in-plane plasmon and the two-magnon mode are two possible candidates. The coupling strength of in-plane plasmon increases upon doping, as shown by the energy-loss function in Ref. 28. Qualitatively, the in-plane plasmon should give a very similar doping effect

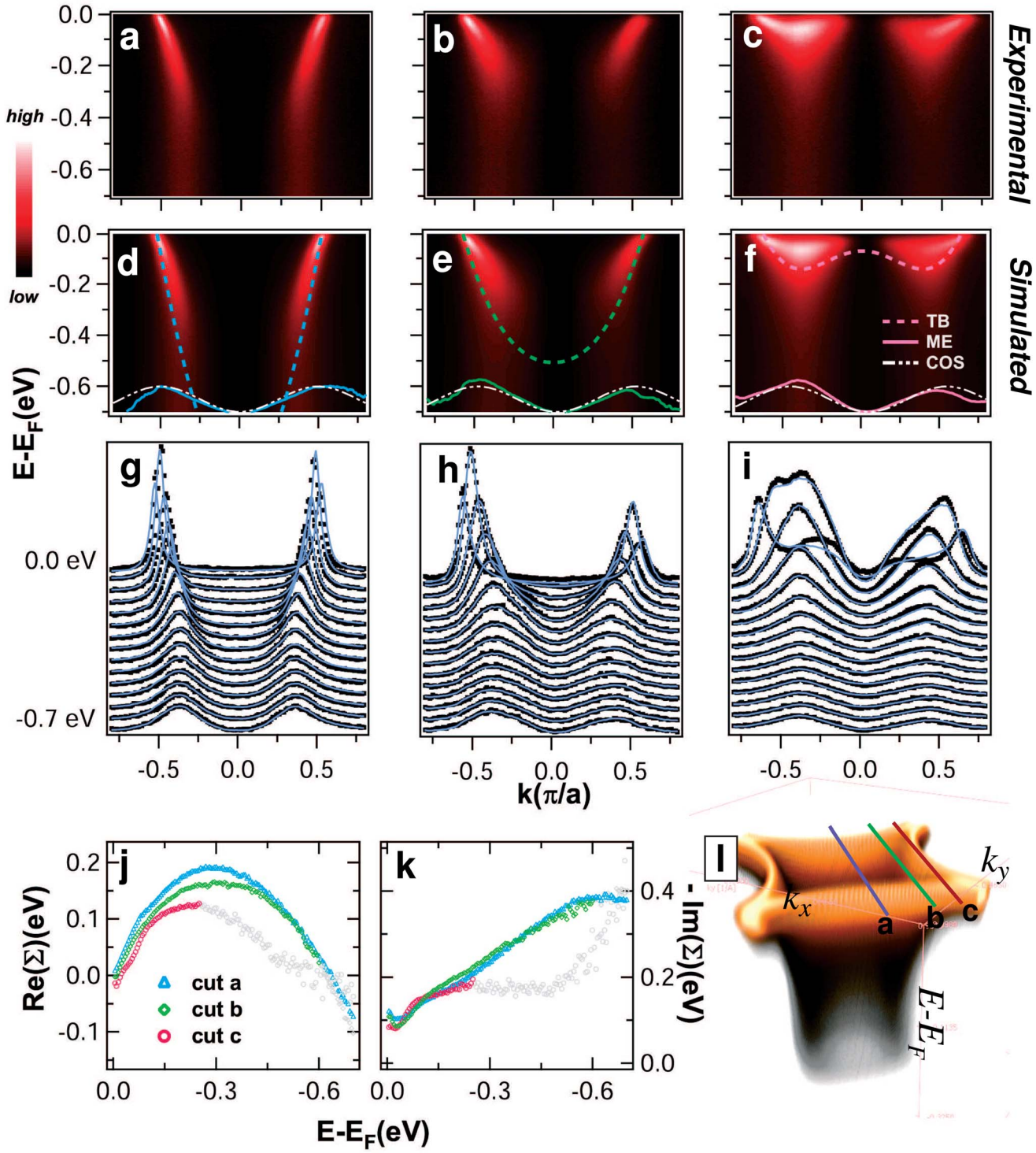

FIG. 6. (Color online) On the first row, (a)–(c) are the experimental ARPES data along the momentum direction as indicated by the band shown in bottom right. On the second row, (d)–(f) are the corresponding simulated images from the 2D analysis. The thicker dashed lines are the dispersions generated from the tight-binding (TB) parameters given above. The solid lines are the matrix elements (ME) obtained from the 2D analysis, where the smaller dashed lines are the empirically guessed form of the matrix element in the form of a cosine function (COS). On the third row, (g)–(i) are the MDCs of raw data (dots) and corresponding simulated images (line). (j) and (k) are the extracted real and imaginary parts of the so-called self-energy in Eq. (A2) for the cuts a, b, and c; the extracted values are plotted in dark symbols to the energy not far from the bottom of the bare band (up to 0.6 eV for cut b and 0.25 eV for cut c) and in light symbols at higher energy. (l) shows the band structure generated from the TB parameters and the loosely called self-energy along the nodal direction.

to that shown in Fig. 4. The problem is that the plasmon mode energy in LSCO is around 0.8 eV or twice as large. On the other hand, the two-magnon mode energy is right in the window for the hole-doped cuprates (0.3–0.4 eV) but not for FO234, electron-doped band (0.5–0.6 eV), while its strength quickly reduces upon doping.[29]

Given the above alternative interpretations and issues related to them, despite the quantitative problem of the HEA size as a function of doping, the anomalous energy scale is still likely caused by the Mott-Hubbard physics. The fact that HEA is absent in FM LSMO (Fig. 5) but present in the Mott-Hubbard system $SrVO_3$ suggests that it is related to antiferromagnetism and Mott-Hubbard physics.

Next is the enhancement of LDA bandwidth which is anomalous because interactions usually reduce the bandwidth. One possible candidate here could be the poor screening effect. With the Hartree-Fock equation of free electron, the Coulomb exchange term without the screening effect[30] will give rise to a negative term which results in an increased bandwidth; the effect of poor screening can be seen in semiconductors. In cuprates, the electrons in lightly doped systems are poorly screened compared to the overdoped regime, and hence the discrepancy of bandwidth is larger in underdoped systems. We note here that, for the $SrVO_3$ system, LDA+DMFT calculation[26] gives the bandwidth correctly. This distinction between $SrVO_3$ and cuprates should be investigated further.

V. CONCLUSION

In conclusion, based on the data from four families of cuprates over a wide doping range, we present evidence of a hierarchy of multiple energy scales in cuprates focused on: the low-energy anomaly of 0.03–0.09 eV, a high-energy anomaly of 0.3–0.5 eV, and an anomalous enhancement of LDA bandwidth, extending over an energy scale of $\approx$2 eV. These results suggest that electron-phonon interaction, short-range Coulomb interaction, and poor screening should be all considered to understand the nature of cuprates.

Note added in proof: Recently, we became aware of other experiments.[31]

ACKNOWLEDGMENTS

We thank A. Macridin, B. Moritz, M. Jarrell, K. M. Shen, D. Scalapino, D. van der Marel, N. J. C. Ingle, and F. Baumberger for helpful discussions. The work at SSRL and ALS are supported by DOE's Office of Basic Energy Sciences under Contracts No. DE-AC02-76SF00515 and No. DE-AC03-76SF00098. The work at Stanford is supported by NSF DMR-0304981 and ONR N00014-04-1-0048. W.M. acknowledges DPST for the financial support. The work at Northeastern is supported by the US DOE Contract No. DE-AC03-76SF00098 and benefited from the allocation of supercomputer time at NERSC and Northeastern's Advanced Scientific Computation Center (ASCC). The work at IOP-CAS is supported by NSF of China. T.P.D. acknowledges ONR N00014-05-1-0127.

APPENDIX: FULL 2D ANALYSIS

In the following, we will show that interestingly, a 2D analysis could describe ARPES data well, covering a large energy and momentum space, by a compact set of parameters. This is an attempt to go beyond the conventional EDC or MDC analysis alone. However, we note that the physical meaning of such a parametrization still remains to be explored.

Here we will apply the 2D analysis on the ARPES data of Pb-substituted Bi2201. The overdoped (OD) samples, $Pb_{0.38}Bi_{1.74}Sr_{1.88}CuO_{6+\delta}$, are nonsuperconducting ($T_c < 4$ K). ARPES data were collected with a photon energy of 42 eV. The energy resolution was set to 18 meV. The linear polarization of the light source is fixed to be in-plane along (0,0) to (π,π) throughout the measurement. Note that the fitted matrix element, which is shown in Figs. 6(d)–6(i), refers to this particular experimental geometry.

The intensity measured in an ARPES experiment on a 2D material here will be parametrized by[2]

$$I(\mathbf{k},\omega) = I_0(\mathbf{k},\nu,\mathbf{A}) f(\omega) \mathcal{A}(\mathbf{k},\omega), \tag{A1}$$

where $I_0(\mathbf{k},\nu,\mathbf{A})$ is proportional to the one-electron matrix element and dependent on the polarization, momentum, and energy of the incoming photon, and $f(\omega)$ is the Fermi function. $\mathcal{A}(\mathbf{k},\omega)$ is the single-particle spectral function given by

$$\mathcal{A}(\mathbf{k},\omega) = \frac{(-1/\pi)\mathrm{Im}\,\Sigma(\mathbf{k},\omega)}{[\omega - \varepsilon_k^0 - \mathrm{Re}\,\Sigma(\mathbf{k},\omega)]^2 + [\mathrm{Im}\,\Sigma(\mathbf{k},\omega)]^2}, \tag{A2}$$

where ϵ_k^0 is the bare band dispersion, and $\Sigma(\mathbf{k},\omega)$ is the self-energy.

We note that we neglect the instrumental resolution here since the feature of interest is large compared to the resolution. In the following, we will assume weak momentum dependence of this extracted self-energy [i.e., $\Sigma(\mathbf{k},\omega) \rightarrow \Sigma(\omega)$].

Figure 6 shows the comparison of the raw ARPES data [first row, Figs. 6(a)–6(c)] and the parametrized data [second row, Fig. 6(d) and 6(e)]. We parametrize the ARPES data with the form given by Eq. (A1) where the spectral function $\mathcal{A}(k,\omega)$ is given by Eq. (A2). In the fitting, we do not assume any form of the self-energy and the matrix element (i.e., every point of the fitted self-energy or matrix element is a free parameter in the fitting procedure.) The bare dispersion used here is the simple form given by the tight-binding (TB) parameters, which is fitted to the LDA calculation shown in Figs. 1(f) and 2. The bare dispersion is given by

$$E(k) = -2t[\cos(k_x a) + \cos(k_y b)] - 2t' \cos(k_x a)\cos(k_y b) - 2t''[\cos(2k_x a) + \cos(2k_y b)] - E_F$$

, where the TB parameters are $t=0.435$, $t'=-0.1$, $t''=0.038$, and $E_F=-0.5231$ eV. For simplicity, we use constant background in the fitting procedure.

The fitting of the ARPES data [Figs. 6(d) and 6(e)] is very well in agreement with average error of $<4\%$. Since the extracted self-energy does not show a strong momentum dependence, the approximate three-dimensional spectra may be generated from this information as shown in Fig. 6(i).

*Electronic address: non@stanford.edu
†Electronic address: zxshen@stanford.edu

[1] Z.-X. Shen, D. S. Dessau, B. O. Wells, D. M. King, W. E. Spicer, A. J. Arko, D. Marshall, L. W. Lombardo, A. Kapitulnik, P. Dickinson, S. Doniach, J. DiCarlo, A. G. Loeser, and C. H. Park, Phys. Rev. Lett. **70**, 1553 (1993).

[2] A. Damascelli, Z. Hussain, and Z.-X. Shen, Rev. Mod. Phys. **75**, 473 (2003).

[3] P. V. Bogdanov, A. Lanzara, S. A. Kellar, X. J. Zhou, E. D. Lu, W. J. Zheng, G. Gu, J.-I. Shimoyama, K. Kishio, H. Ikeda, R. Yoshizaki, Z. Hussain, and Z. X. Shen, Phys. Rev. Lett. **85**, 2581 (2000).

[4] A. Kaminski, M. Randeria, J. C. Campuzano, M. R. Norman, H. Fretwell, J. Mesot, T. Sato, T. Takahashi, and K. Kadowaki, Phys. Rev. Lett. **86**, 1070 (2001).

[5] P. D. Johnson, T. Valla, A. V. Fedorov, Z. Yusof, B. O. Wells, Q. Li, A. R. Moodenbaugh, G. D. Gu, N. Koshizuka, C. Kendziora, Sha Jian, and D. G. Hinks, Phys. Rev. Lett. **87**, 177007 (2001).

[6] A. Lanzara, P. V. Bogdanov, X. J. Zhou, S. A. Kellar, D. L. Feng, E. D. Lu, T. Yoshida, H. Eisaki, A. Fujimori, K. Kishio, J.-I. Shimoyama, T. Nodak, S. Uchidak, Z. Hussain, and Z.-X. Shen, Nature (London) **412**, 510 (2001).

[7] X. J. Zhou, T. Yoshida, A. Lanzara, P. V. Bogdanov, S. A. Kellar, K. M. Shen, W. L. Yang, F. Ronning, T. Sasagawa, T. Kakeshita, T. Noda, H. Eisaki, S. Uchida, C. T. Lin, F. Zhou, J. W. Xiong, W. X. Ti, Z. X. Zhao, A. Fujimori, Z. Hussain, and Z.-X. Shen, Nature (London) **423**, 398 (2003).

[8] T. Cuk, F. Baumberger, D. H. Lu, N. Ingle, X. J. Zhou, H. Eisaki, N. Kaneko, Z. Hussain, T. P. Devereaux, N. Nagaosa, and Z.-X. Shen, Phys. Rev. Lett. **93**, 117003 (2004).

[9] X. J. Zhou, Junren Shi, T. Yoshida, T. Cuk, W. L. Yang, V. Brouet, J. Nakamura, N. Mannella, Seiki Komiya, Yoichi Ando, F. Zhou, W. X. Ti, J. W. Xiong, Z. X. Zhao, T. Sasagawa, T. Kakeshita, H. Eisaki, S. Uchida, A. Fujimori, Zhenyu Zhang, E. W. Plummer, R. B. Laughlin, Z. Hussain, and Z.-X. Shen, Phys. Rev. Lett. **95**, 117001 (2005).

[10] W. Meevasana, N. J. C. Ingle, D. H. Lu, J. R. Shi, F. Baumberger, K. M. Shen, W. S. Lee, T. Cuk, H. Eisaki, T. P. Devereaux, N. Nagaosa, J. Zaanen, and Z.-X. Shen, Phys. Rev. Lett. **96**, 157003 (2006).

[11] M. C. Schabel, C.-H. Park, A. Matsuura, Z.-X. Shen, D. A. Bonn, X. Liang, and W. N. Hardy, Phys. Rev. B **57**, 6090 (1998).

[12] R. Hayn, H. Rosner, V. Yu. Yushankhai, S. Haffner, C. Durr, M. Knupfer, G. Krabbes, M. S. Golden, J. Fink, H. Eschrig, D. J. Singh, N. T. Hien, A. A. Menovsky, Ch. Jung, and G. Reichardt, Phys. Rev. B **60**, 645 (1999).

[13] H. Lin, S. Sahrakorpi, R. S. Markiewicz, and A. Bansil, Phys. Rev. Lett. **96**, 097001 (2006).

[14] Y. Chen, Akira Iyo, Wanli Yang, Xingjiang Zhou, Donghui Lu, Hiroshi Eisaki, Thomas P. Devereaux, Zahid Hussain, and Z.-X. Shen, Phys. Rev. Lett. **97**, 236401 (2006).

[15] S. Sahrakorpi, M. Lindroos, R. S. Markiewicz, and A. Bansil, Phys. Rev. Lett. **95**, 157601 (2005).

[16] T. Greber, T. J. Kreutz, and J. Osterwalder, Phys. Rev. Lett. **79**, 4465 (1997).

[17] In examining various published band structures of Bi2201 and Bi2212 (see, e.g., references cited below), we find that the LDA in all cases gives a *lower* binding energy for band B than the experimental value; V. Bellini, F. Manghi, T. Thonhauser, and C. Ambrosch-Draxl, Phys. Rev. B **69**, 184508 (2004); D. J. Singh and W. E. Pickett, *ibid.* **51**, 3128 (1995); M. S. Hybertsen and L. F. Mattheiss, Phys. Rev. Lett. **60**, 1661 (1988); P. A. Sterne and C. S. Wang, J. Phys. C **21**, L949 (1988).

[18] F. Ronning, K. M. Shen, N. P. Armitage, A. Damascelli, D. H. Lu, Z.-X. Shen, L. L. Miller, and C. Kim, Phys. Rev. B **71**, 094518 (2005).

[19] D. van der Marel, H. J. A. Molegraaf, J. Zaanen, Z. Nussinov, F. Carbone1, A. Damascelli, H. Eisaki, M. Greven, P. H. Kes, and M. Li, Nature (London) **425**, 271 (2003).

[20] M. R. Norman and A. V. Chubukov, Phys. Rev. B **73**, 140501(R) (2006).

[21] N. Mannella, W. L. Yang, X. J. Zhou, H. Zheng, J. F. Mitchell, J. Zaanen1, T. P. Devereaux, N. Nagaosa, Z. Hussain, and Z.-X. Shen, Nature (London) **438**, 474 (2005).

[22] K. M. Shen, F. Ronning, D. H. Lu, W. S. Lee, N. J. C. Ingle, W. Meevasana, F. Baumberger, A. Damascelli, N. P. Armitage, L. L. Miller, Y. Kohsaka, M. Azuma, M. Takano, H. Takagi, and Z.-X. Shen, Phys. Rev. Lett. **93**, 267002 (2004).

[23] E. Dagotto, A. Nazarenko, and M. Boninsegni, Phys. Rev. Lett. **73**, 728 (1994).

[24] A. Macridin, B. Moritz, T. Devereaux, and M. Jarell (private communication); Alexandru Macridin, M. Jarrell, Thomas Maier, and D. J. Scalapino, arXiv:cond-mat/0701429 (unpublished).

[25] T. Yoshida, K. Tanaka, H. Yagi, A. Ino, H. Eisaki, A. Fujimori, and Z.-X. Shen, Phys. Rev. Lett. **95**, 146404 (2005).

[26] I. A. Nekrasov, K. Held, G. Keller, D. E. Kondakov, Th. Pruschke, M. Kollar, O. K. Andersen, V. I. Anisimov, and D. Vollhardt, Phys. Rev. B **73**, 155112 (2006).

[27] J. K. Freericks, T. P. Devereaux, R. Bulla, and Th. Pruschke, Phys. Rev. B **67**, 155102 (2003).

[28] S. Uchida, T. Ido, H. Takagi, T. Arima, Y. Tokura, and S. Tajima, Phys. Rev. B **43**, 7942 (1991).

[29] S. Sugai, H. Suzuki, Y. Takayanagi, T. Hosokawa, and N. Hayamizu, Phys. Rev. B **68**, 184504 (2003).

[30] N. W. Ashcroft and N. D. Mermin, *Solid State Physics* (Harcourt, Orlando, 1976), Chap. 17, pp. 334–337.

[31] J. Graf, G.-H. Gweon, K. McElroy, S. Y. Zhou, C. Jozwiak, E. Rotenberg, A. Bill, T. Sasagawa, H. Eisaki, S. Uchida, H. Takagi, D.-H. Lee, and A. Lanzara, Phys. Rev. Lett. **98**, 067004 (2007); B. P. Xie, K. Yang, D. W. Shen, J. F. Zhao, H. W. Ou, J. Wei, S. Y. Gu, M. Arita, S. Qiao, H. Namatame, M. Taniguchi, N. Kaneko, H. Eisaki, Z. Q. Yang, and D. L. Feng, Phys. Rev. Lett. **98**, 147001 (2007); T. Valla, T. E. Kidd, Z.-H. Pan, A. V. Fedorov, W.-G. Yin, G. D. Gu, and P. D. Johnson, arXiv:cond-mat/0610249 (unpublished); Z.-H. Pan, P. Richard, A. V. Fedorov, T. Kondo, T. Takeuchi, S. L. Li, Pengcheng Dai, G. D. Gu, W. Ku, Z. Wang, and H. Ding, arXiv:cond-mat/0610442 (unpublished); J. Chang, S. Pailhes, M. Shi, M. Månsson, T. Claesson, O. Tjernberg, J. Voigt, V. Perez-Dieste, L. Patthey, N. Momono, M. Oda, M. Ido, A. Schnyder, C. Mudry, and J. Mesot, arXiv:cond-mat/0610880 (unpublished); J. Hwang, E. J. Nicol, T. Timusk, A. Knigavko, and J. P. Carbotte, arXiv:cond-mat/0610488 (unpublished).